DOI: 10.1002/chem.201103096

Assessing Metal–Metal Multiple Bonds in Cr−Cr, Mo−Mo, and W−W Compounds and a Hypothetical U−U Compound: A Quantum Chemical Study Comparing DFT and Multireference Methods

Giovanni Li Manni,[a] Allison L. Dzubak,[b] Abbas Mulla,[b] David W. Brogden,[c] John F. Berry,*[c] and Laura Gagliardi*[b]

Abstract: To gain insights into the trends in metal–metal multiple bonding among the Group 6 elements, density functional theory has been employed in combination with multiconfigurational methods (CASSCF and CASPT2) to investigate a selection of bimetallic, multiply bonded compounds. For the compound [Ar-MM-Ar] (Ar = 2,6-$(C_6H_5)_2$-C_6H_3, M = Cr, Mo, W) the effect of the Ar ligand on the M_2 core has been compared with the analogous [Ph-MM-Ph] (Ph = phenyl, M = Cr, Mo, W) compounds. A set of $[M_2(dpa)_4]$ (dpa = 2,2′-dipyridylamide, M = Cr, Mo, W, U) compounds has also been investigated. All of the compounds studied here show important multiconfigurational behavior. For the Mo_2 and W_2 compounds, the $\sigma^2\pi^4\delta^2$ configuration dominates the ground-state wavefunction, contributing at least 75%. The Cr_2 compounds show a more nuanced electronic structure, with many configurations contributing to the ground state. For the Cr, Mo, and W compounds the electronic absorption spectra have been studied, combining density functional theory and multireference methods to make absorption feature assignments. In all cases, the main features observed in the visible spectra may be assigned as charge-transfer bands. For all compounds investigated the Mayer bond order (MBO) and the effective bond order (EBO) were calculated by density functional theory and CASSCF methods, respectively. The MBO and EBO values share a similar trend toward higher values at shorter normalized metal–metal bond lengths.

Keywords: bond theory · density functional calculations · electronic states · metal–metal interactions · quantum chemistry

Introduction

Ever since the discovery of the multiple metal–metal bond in $[Re_2Cl_8]^{2-}$,[1,2] there has been a considerable amount of research dedicated to metal–metal multiple bonding. Electron-rich metal–metal units are of general interest because of their unique electronic and optical properties.[3] Several new examples of metal–metal multiply bonded compounds incorporating the Group 6 metals have recently been of interest. For example, various groups have shown interest in oligothiophene compounds incorporating metal–metal multiple bonds because of their potential applications in optoelectronic and magnetic devices. Burdzinski et al.[4] recently prepared oligomers of empirical formula $[Mo_2(TiPB)_2$-$(O_2C(Th)$-$C_4(n\text{-hexyl})_2S$-$(Th)CO_2)]$ (TiPB = 2,4,6-triisopropyl benzoate; Th = thiophene) and compounds of formulae *trans*-$[Mo_2(TiPB)_2L_2]$ in which L = Th, BTh (Bth = 2,2′-bithiophene-5-carboxylate) and TTh (the corresponding thienylcarboxylate), which are considered as models for the oligomers. The X-ray analysis of *trans*-$[Mo_2(TiPB)_2BTh_2]$ (**1**; Figure 1) revealed the presence of $L\pi^*$–$M_2\delta$–$L\pi^*$ conjugation, and density functional theory (DFT) calculations indicated that the HOMO is mainly a M_2 δ orbital and the LUMO is mainly based on the thienylcarboxylate π* orbitals.

Burdzinski et al.[4] studied also the photophysical properties of these oligomers, which showed relatively slow metal-to-ligand charge-transfer (MLCT) triplet intersystem crossing compared to the majority of second- and third-row transition metal complexes. They noticed that the ^{1}MLCT–^{3}MLCT gap is relatively small in the Mo complexes, suggesting a large mixing of the metal δ and organic π systems. These Mo_2-based oligothiophenes have thus a unique metal-based triplet emission.

[a] G. Li Manni
Department of Physical Chemistry, University of Geneva
30, q. E. Ansermet, 1211 Genève (Switzerland)

[b] A. L. Dzubak, A. Mulla, Prof. L. Gagliardi
Department of Chemistry,
University of Minnesota and Minnesota Supercomputing Institute
207 Pleasant St. SE, Minneapolis, MN 55455 (USA)
E-mail: gagliard@umn.edu

[c] D. W. Brogden, Prof. J. F. Berry
Department of Chemistry, University of Wisconsin—Madison
1101 University Ave. Madison, WI 53706 (SA)
E-mail: berry@chem.wisc.edu

Supporting information for this article is available on the WWW under http://dx.doi.org/10.1002/chem.201103096. Additional details of the calculations: cartesian coordinates; total electronic energies and molecular orbitals and electronic spectra.

 © 2012 Wiley-VCH Verlag GmbH & Co. KGaA, Weinheim

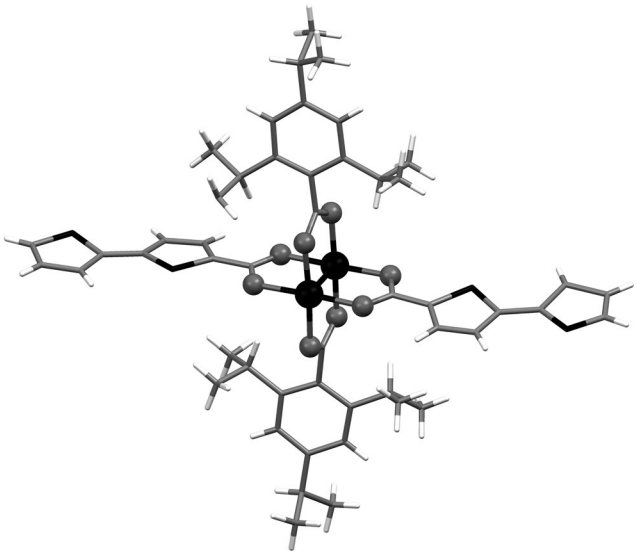

Figure 1. Experimentally determined structure of compound **1**. Color code: C = gray-capped stick, H = white-capped stick, S = black-capped stick, Mo = black ball, O = gray ball.

Alberding et al.[3] prepared the $[MM'(TiPB)_4]$ compounds, in which M = Mo or W and M′ = W and characterized them with various techniques. Electronic absorption, steady-state emission and transient absorption spectroscopy indicate that these compounds have strong absorptions in the visible region that are assigned to MM′ δ to arylcarboxylate π* transitions, ^{1}MLCT. Luminescence from two excited states also occurs, which are assigned as the ^{1}MLCT and ^{3}MM′ δ–δ* states.

Nippe et al.[5] reported the synthesis of $[W_2(dpa)_4]$ (dpa = 2,2′-dipyridylamide) (**2c**) (Figure 2) and its characterization by X-ray crystallography and cyclic-voltammetry. They compared it with its earlier reported molybdenum analogue, $[Mo_2(dpa)_4]$ (**2b**).[6] They also synthesized one-electron oxidation products of $[W_2(dpa)_4]$ and $[Mo_2(dpa)_4]$, namely $[W_2(dpa)_4][BPh_4]$ and $[Mo_2(dpa)_4][BPh_4]$ (BPh_4 = tetraphenylborate). The crystallographically determined metal–metal distances of 2.23 and 2.14 Å in $[W_2(dpa)_4][BPh_4]$ and $[Mo_2(dpa)_4][BPh_4]$, respectively, are in agreement with metal–metal bond orders of 3.5. The molecules $[W_2(dpa)_4]$ and $[Mo_2(dpa)_4]$ have been utilized along with the $[Cr_2(dpa)_4]$ analogue (**2a**) to prepare linear, trinuclear heterometallic molecules with an M≡M···M′ chain, with M = Cr, Mo, or W, and M′ = Cr, Mn, Fe, Co, Ni, and Zn.[7–11] The heterometallic molecules show rich optical and redox properties, and a better understanding of these properties can be greatly facilitated by a quantum chemical analysis of the Cr_2, Mo_2, and W_2 precursor molecules.

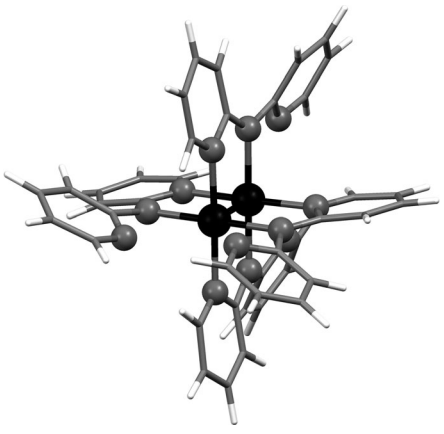

Figure 2. The experimental structure of compound **2c**. Color code: C = gray-capped stick, H = white-capped stick, W = black ball, N = gray ball.

We have studied metal–metal multiple bonds in the Cr_2, Mo_2, and W_2 dimers by making use of the concept of effective bond order (EBO)[14,15] that arises from a multiconfigurational complete active space-SCF (CASSCF) wavefunction.[16] We have demonstrated that a sextuple bond exists in Mo_2 and W_2, but hardly in Cr_2.[14,17] The weakness of the Cr–Cr bond is related to the difference in size between the 3d and 4s orbitals. The 4s–4s interaction occurs at a considerably longer distance than the 3d–3d interaction. This unbalance weakens the 3d bonds and makes the 4s–4s interaction repulsive at equilibrium geometry. Another important factor is the repulsive interaction between the closed 3p shells, which have about the same radial extension as the 3d orbitals. The unbalance between the s and d orbitals decreases for second-row transition metals and even more for the third row. Moreover, relativistic effects play an important role in making the two sets of orbitals more equal in size, which overall enhance the bond strength of the diatomics. Various low-valent Cr–Cr complexes recently synthesized present a multiple bond that, despite changes in the nature of the ligand or with the oxidation state of the Cr atom, yield EBO values in the relatively narrow range between 3.4 and 3.9 that correlate roughly with the Cr–Cr bond length.[18] In order to protect the dimetallic unit from possible oxidation or oligomerization, terphenyl ligands, the skeleton structure of which is 2,6-$(C_6H_5)_2$-C_6H_3 (Ar), have been employed to embed the metal dimer. Experimental and theoretical works have also shown that [Ar′-CrCr-Ar′] (**3a**, Scheme 1) (Ar′ = 2,6-(2,6-*i*Pr_2-C_6H_3)$_2$-C_6H_3) features a *trans*-bent geometry.[15,19–21] Since the Ar ligand successfully stabilizes dimers of main group elements and the Cr dimer, its capabilities in protecting dimers of Fe and Co were also investigated.[22,23] The flanking aryl/metal η^6 interaction makes the Fe–Fe and Co–Co bonds longer than in other compounds. In order to quantify the influence of the flank-

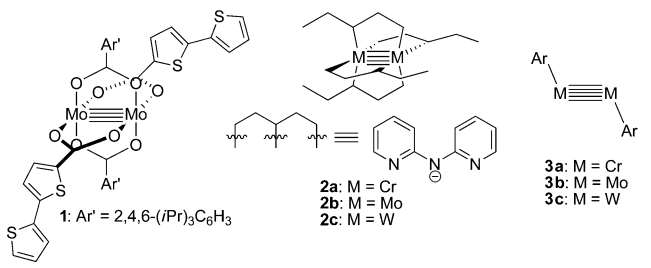

Scheme 1. Compounds studied in this work.

 © 2012 Wiley-VCH Verlag GmbH & Co. KGaA, Weinheim

ing aryl ring on the M–M bond, several simplified model systems containing a Co–Co and Fe–Fe core unit, but without ligands capable of giving η^6 interactions, were studied by DFT and CASSCF followed by perturbation theory to second order (CASPT2) and compared to the complexes featuring the η^6 interaction computed at the same level of theory.[21]

In this paper we report the results of the study of several compounds containing Cr–Cr, Mo–Mo and W–W multiple bonds to reveal and interpret any generalized trends that may be present. First we will describe the *trans*-bent molecules [Ar-MM-Ar] (**3a**, M=Cr; **3b**, M=Mo; **3c**, M=W), for which the Mo and W analogs have not yet been synthesized up to date and have, to our knowledge, never been the subject of computational investigation. The effect of the Ar ligand on the different bimetallic units will be discussed and compared with the effect of phenyl (Ph) in the analogous [Ph-MM-Ph] compounds.

In the second part of the paper we will focus on the compounds synthesized by Burdzinski et al.[4] and Nippe et al.,[5] compounds **1** and **2**, respectively. We will report the results of our theoretical calculations on the Mo–Mo type **1** compound. For compounds **2** we will discuss the Cr–Cr, Mo–Mo and W–W species, **2a**, **2b**, and **2c**, respectively. In all cases our results will be compared with experimental data. Finally, we will discuss the hypothetical U–U equivalent of **2**, which, if synthesized, would represent a breakthrough in diuranium chemistry.[24–26] The aim of this study is to understand the nature of the metal–metal bonds in these compounds by a multiconfigurational quantum chemical characterization, inspect the most significant spectroscopic transitions and predict whether compound of type **2** containing a U–U unit could also exist. Where possible, we include results from DFT calculations in addition to the CASPT2 results, so that comparisons between the two methods may be made. We also include a discussion of calculated metal–metal bond orders, which are particularly problematic since computations typically yield non-integer bond orders that differ significantly from what one expects from simple molecular orbital theory.

Computational Methods

The [Ph-MM-Ph] and [Ar-MM-Ar] species (M=Cr, Mo, W): Initial geometry optimizations were performed at the DFT level of theory using the TURBOMOLE quantum chemistry software.[27] The PBE functional[28] was employed along with the triple-zeta valence plus polarization (def-TZVP) basis set on all the atoms. Vibrational frequency calculations were also performed in order to verify the nature of the stationary points. All structures reported in this study are local minima with all real frequencies, with the exception of the Ph-MM-Ph compounds, which exhibit two imaginary frequencies. Even if the planar [Ph-MM-Ph] structures are not local minima, we decided to characterize their electronic structure in order to compare them with the [Ar-MM-Ar] analogues. The DFT-optimized coordinates are reported in the Supporting Information for all the systems described in this study.

The multiconfigurational complete active space-SCF method[29] followed by second-order perturbation theory (CASSCF/CASPT2)[30] was employed to re-optimize selected bond lengths, namely the M–M (M=Cr, Mo and W) and M–C bonds. A numerical optimization procedure was employed, which consisted of varying the M–M and M–C distances, optimizing the structures at the DFT level while keeping the M–M and M–C distances fixed, and performing CASPT2 calculations at these geometries. Numerical gradients and hessians on the CASPT2 potential-energy surfaces were then computed to check the nature of the stationary points.

The CASSCF/CASPT2 calculations were performed using the MOLCAS-7.3 package.[31] Basis sets of the atomic natural orbital type[32,33] with triple-zeta plus polarization quality (ANO-RCC-VTZP) were used for the transition metal atoms, whereas basis sets of double-zeta basis set quality (ANO-RCC-VDZP) were used for the other atoms. Scalar relativistic effects were included using the Douglas–Kroll–Hess Hamiltonian.[34] The two-electron integral evaluation was simplified by employing the Cholesky decomposition technique.[35–37] The decomposition threshold was chosen to be 10^{-4}, as this should correspond to an accuracy in total energies of the order of mHartree or higher. At the CASPT2 level of theory the frozen natural orbital approach with 70% of the virtual orbitals taken into account was applied (FNO-CASPT2) to reduce the computational costs.[38] In order to prevent weak intruder states an imaginary shift of 0.2 units was added to the external part of the zero-order Hamiltonian. For all the investigated species, at the CASPT2 level, the 1s orbitals for all C atoms were kept frozen; moreover, for the [Ph-MoMo-Ph] compound orbitals up to and including the 3d for Mo atoms were kept frozen; for [Ph-WW-Ph] compound orbitals up to and including 4d for W atoms were kept frozen; for the [Ar-CrCr-Ar] only orbitals up to 2p for Cr were kept frozen, whereas for [Ar-MoMo-Ar] and [Ar-WW-Ar] orbitals up to 3d and 4d, respectively, were kept frozen. At the CASSCF level, for all the species the active space contains 14 electrons distributed in 14 orbitals, CAS(14,14). This active space comprises all the nd (n=3, 4, or 5) orbitals forming the M–M multiple bond as well as two bonding and two antibonding orbitals describing the M–C interaction. Six active electrons come from each M atom, corresponding to the valence configuration $n\mathrm{d}^5\,(n+1)\mathrm{s}^1$ (n=3, 4, and 5), and one electron comes from each C atom bonded to the transition metal, adding up to 14 electrons in total.

Calculations were performed on the ^1A_g ground state. In the [Ph-MM-Ph] calculations the geometries of the systems were constrained to C_{2h} symmetry, while in the [Ar-MM-Ar] calculations they were constrained to C_2 symmetry. For all species under investigation we have computed the effective bond order (EBO)[14,39] which quantifies the formation of a chemical bond from CASSCF wavefunctions. For a single bond the EBO is given by Equation (1), in which η_b and η_{ab} are the sums of the occupation numbers of the bonding and anti-bonding molecular orbital pair derived from the CASSCF wavefunction.

$$\mathrm{EBO} = (\eta_b - \eta_{ab})/2 \qquad (1)$$

In multiply bonded systems one has to add up the individual values generated from the various pairs of bonding and antibonding orbitals (e.g., σ, π, and δ) to obtain the total EBO. Note that η_b and η_{ab} can assume any value between zero and two and are not necessarily integer numbers. Equation (1) thus implies that the EBO value will always be lower or at most equal to the bond order that one obtains from conventional molecular orbital theory, for which the orbitals have an occupation number always equal to either 2, 1, or 0.

There are various ways of quantifying bond orders.[40–42] The EBO concept relies on a multiconfigurational wavefunction and takes into account the effect of electron correlation involving the antibonding orbitals. Moreover, if used in combination with ANO basis sets optimized for multiconfigurational calculations (as done in this study), it provides stable values.

We have previously employed the CASSCF/CASPT2 approach to study several metal–metal multiply bonded species like the $[Re_2Cl_8]^{2-}$ system,[43] the octamethyldimetalate compounds of Cr^{II}, Mo^{II}, W^{II}, and Re^{III},[44] the octabromoditechnetate(III) compound[45] and the triply bonded $[Tc_2X_4(PMe_3)_4]$ (X=Cl, Br) complexes.[46] In all cases the approach has proven to be successful in describing the electronic structure

 © 2012 Wiley-VCH Verlag GmbH & Co. KGaA, Weinheim

of such compounds and the metal–metal multiple bond, because of its ability to describe the electronic structure of multiconfigurational species.

The Burdzinski Mo−Mo species: The original coordinates of **1** were obtained from the X-ray data.[4] In our calculations, the TiPB ligands were replaced with formate groups and the BTh groups with the simpler Th ones; this approximation was found to be adequate, because the external groups play mainly a steric role. As already discussed in reference [4] the extension of the length of the thienyl groups may, on the other hand, affect the electronic structure of the Mo−Mo unit. In this context, however, we decided to focus on the simplest case. The reduced structure (Figure 3) was used for all subsequent calculations. The molecule has C_{2h} symmetry, which was maintained throughout all calculations.

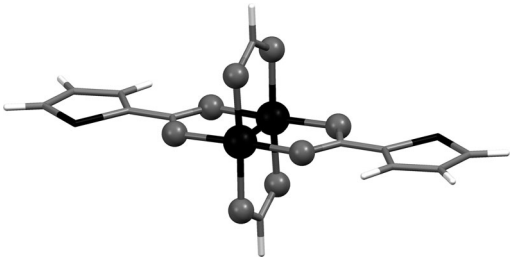

Figure 3. Simplified structure of **1** used for all calculations. Color code: C = gray capped stick, H = white capped stick, S = black capped stick, Mo = black ball, O = gray ball.

A DFT geometry optimization was performed for the singlet ground state using the PBE functional and the Stuttgart RSC 1997 ECP basis set, within Gaussian 09.[47] Subsequent CASSCF/CASPT2 single-point calculations (with ANO-RCC-VTZP type basis sets) were performed at the PBE-optimized geometry. The Mo−Mo bond was successively re-optimized at the CASPT2 level by using a numerical optimization procedure, analogous to the one described in the previous section. Several CASSCF calculations were initially performed in order to select the appropriate active space for this system and it was found that a reasonable active space for the ground state consists of eight active electrons in eight active orbitals. These orbitals are bonding and antibonding linear combinations of Mo 4d orbitals with σ, π and δ symmetry (the Results section for a detailed description) and they are localized on the Mo_2 unit. The two remaining MOs arising from the linear combination of the fifth 4d orbital on each Mo atom were not included in the active space because they are not in the HOMO–LUMO region and they are mainly metal–ligand orbitals. No metal–ligand (M–L) orbitals were included in the active space. In the [Ar-MM-Ar] case, it was not an issue of computational cost to include the M–L bonding and antibonding orbitals. In this case, on the other hand, including the M–L bonding and antibonding orbitals would add at least 16 orbitals to the active space, which would not be computationally tractable. The smaller active space of eight in eight is still satisfactory, as the multiconfigurational character is mainly localized in the Mo_2 unit and the M–L interaction can be adequately treated at the subsequent PT2 level. The lowest excited singlet and triplet states were also computed.

$[M_2(dpa)_4]$ (M = Cr, Mo, W) species: Initial coordinates for the geometry optimization of $[Cr_2(dpa)_4]$ (**2a**) were obtained from the crystallographic data for the compound in its crystal form that contains no solvent molecules.[41] Initial coordinates of $[Mo_2(dpa)_4]$ (**2b**) were obtained from reference [6] and initial coordinates for $[W_2(dpa)_4]$ (**2c**) were obtained from the Supporting Information of reference [5]. Geometry optimization and frequency calculations for **2a–c** were performed using the TURBOMOLE software package and the PBE functional. The def2-TZVP basis set was employed for N, Cr, Mo, and W atoms and the SV(P) basis set was used for all other atoms. In the CASSCF/CASPT2 calculations an ANO-RCC-TZVP basis set was used for N, Cr, Mo, and W, and the ANO-RCC-DZVP basis set was used for all other atoms. The molecules have C_2 symmetry, which was maintained throughout all calculations, except the $[Cr_2(dpa)_4]$ geometry optimization, for which D_2 symmetry was imposed. Molecular orbitals included in the active space are reported in the Supporting Information. TD-DFT calculations were performed using Gaussian 09, Revision B.01[47] using the PBE functional. The Stuttgart–Dresden electron core potential (SDD) was used for Cr, Mo, and W atoms. The TZVP basis set was employed for C and N atoms, and the SVP basis set for H atoms. Compositions of molecular orbitals and Mayer bond orders were calculated using the AOmix program.[48,49]

In the CASSCF calculations an active space of eight electrons in eight orbitals was chosen in analogy with the Burdzinski Mo−Mo calculation. These orbitals are linear combinations of 3d, 4d, and 5d orbitals with σ, π and δ symmetry for $[Cr_2(dpa)_4]$, $[Mo_2(dpa)_4]$ and $[W_2(dpa)_4]$, respectively (see the Results section for a detailed description). Also in this case two MOs arising from the 4d orbitals were not included in the active space, because they are not in the HOMO–LUMO region and they are delocalized between the metal and the ligand. Due to the larger than normal discrepancy of the DFT bond length with experiment, we optimized the W−W bond length at the CASPT2 level by following the same numerical procedure as for the other compounds. We computed several singlet and triplet excitations and their intensity, including spin-orbit coupling among the various states. The intensities and spin-orbit coupling were determined by employing the complete active space state interaction method, CASSI[50] which employs an effective one-electron spin-orbit (SO) Hamiltonian, based on the mean field approximation of the two electronic parts.[51]

Results

[Ph-MM-Ph] (M = Cr, Mo, W): The most relevant structural parameters of the DFT- and CASPT2-optimized [Ph-MM-Ph] systems in their ^1A_g ground state are reported in Table 1. Figure 4 depicts the DFT-optimized structure of [Ph-MoMo-Ph], the CrCr and WW analogues look similar. DFT predicts the Mo−Mo and W−W bond lengths to be 0.05 and 0.07 Å, respectively, longer compared to the corresponding CASPT2 values. The DFT and CASPT2 M−C predicted bond lengths differ by at most 0.01 Å.

Table 1. Most significant structural parameters , and bond order for the [Ph-MM-Ph] systems.

System/Theory	M−M [Å]	M−C [Å]	M-M-C [°]	EBO/ Mayer BO[b]
[Ph-CrCr-Ph]/DFT[a]	1.707	2.033	94.3	
[Ph-CrCr-Ph]/CASPT2[a]	1.752	2.018	88.4	3.52
[Ph-MoMo-Ph]/DFT	2.059	2.098	97.9	4.55
[Ph-MoMo-Ph]/CASPT2	2.010	2.107	97.3	4.26
[Ph-WW-Ph]/DFT	2.154	2.087	100.4	4.57
[Ph-WW-Ph]/CASPT2	2.080	2.097	99.4	4.32

[a] From references [15,21]. [b] Mayer bond order from DFT and EBO from CASPT2.

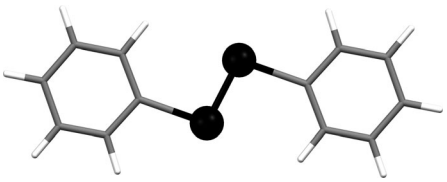

Figure 4. DFT structure of [Ph-MoMo-Ph]; Color code: C = gray capped stick, H = white capped stick, Mo = black ball.

© 2012 Wiley-VCH Verlag GmbH & Co. KGaA, Weinheim

For [Ph-MoMo-Ph] the CASSCF calculation predicted natural orbital occupation numbers reported in the Supporting Information, which provide an EBO of 4.26. Inspection of the multideterminantal CASSCF wavefunction shows that the closed shell configuration, $\sigma_g^2\pi_u^4\delta_g^4$, dominates with a weight of 68%, which corresponds to a formal quintuple bond. A few other configurations contribute with weights lower than 5%; which correspond to double excitations from the bonding orbitals to their antibonding counterparts. For [Ph-WW-Ph], natural orbitals are reported in the Supporting Information with an EBO equal to 4.32. The closed shell $\sigma_g^2\pi_u^4\delta_g^4$ configuration, corresponding to a formal quintuple bond, is also dominant in this case with a weight of about 70%. The EBO for [Ph-CrCr-Ph] reported in our prior studies[15,21] is equal to 3.52 and in this case the closed shell configuration has a weight of only 45%. In the Mo–Mo and W–W compounds the calculated metal–metal bond order is about one unit larger than in the corresponding Cr–Cr compound. The same trend occurs in the diatomic molecules.[14]

[Ar-MM-Ar] (M = Cr, Mo, W) systems: While [Ar′-CrCr-Ar′] (**3a**) (Ar′ = 2,6-(2,6-*i*Pr$_2$-C$_6$H$_3$)$_2$-C$_6$H$_3$) has been synthesized,[19] the MoMo and WW analogues, **3b** and **3c**, have not been synthesized to date. In our study we employed Ar (2,6-(C$_6$H$_5$)$_2$-C$_6$H$_3$) as a simplified model for Ar′. Vibrational frequency analysis indicates that all three [Ar-MM-Ar] compounds are local minima on their potential-energy surface.

The most relevant structural parameters of the DFT- and CASPT2-optimized [Ar-MM-Ar] compounds in their ^1A_g ground state are reported in Table 2. Figure 5 depicts the DFT-optimized structure of **3a**; **3b** and **3c** analogues look similar.

The DFT value for the Cr–Cr distance in **3a** is about 0.1 Å shorter than the experimental value, while the CASPT2 Cr–Cr distance is in better agreement with experiment. The structure of **3a** was fully optimized at the DFT level by imposing only the constraints of C_2 symmetry instead of C_{2h}, and this is the reason why the DFT-optimized structure has a nonplanar C-Cr-Cr-C dihedral angle. On the other hand, CASPT2 predicts the structure with the planar C-Cr-Cr-C dihedral angle to lie 11.5 kJ mol^{-1} lower in energy than the structure with the dihedral angle of 166.7 (the DFT-relaxed structure with the M–M and M–C fixed).

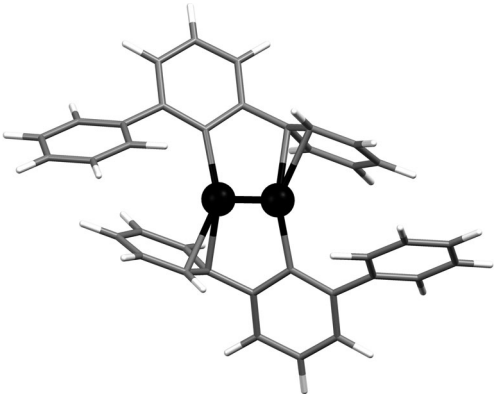

Figure 5. DFT structure of [Ar-CrCr-Ar]; Color code: C = gray capped stick, H = white capped stick, Cr = black ball.

Overall the potential-energy surface for [Ar-CrCr-Ar] is quite flat both along the Cr–Cr coordinate and also the Cr–C coordinate.

The occupation numbers for the natural orbitals (reported in Supporting Information) that make up the Cr–Cr bond provide an EBO of 3.07, similar to what is found for [Ph-CrCr-Ph]. The closed shell configuration, $\sigma_g^2\pi_u^4\delta_g^4$, corresponding to a formal quintuple bond, appears in the multiconfigurational wavefunction with a weight of only 33%. The second most important configuration, $\sigma_g^2\pi_u^4\delta_g^2\delta_u^2$, has a weight of 8%.

For **3b**, DFT predicts a Mo–Mo bond length almost 0.5 Å longer than CASPT2. This difference is mostly due to the fact that DFT predicts a strong Mo–aryl η^6 interaction, while CASSCF and CASPT2 predict a weaker one. The CASSCF molecular orbitals are not delocalized between the Mo and aryl fragments. The occupation numbers for the natural orbitals (reported in Supporting Information) that make up the Mo–Mo bond provide an EBO of 4.3, similar to that found for [Ph-MoMo-Ph]. The closed shell configuration, $\sigma_g^2\pi_u^4\delta_g^4$, corresponding to a formal quintuple bond, dominates the multiconfigurational wavefunction with a weight of 70%. Overall the potential-energy surface for [Ar-MoMo-Ar] is less flat both along the Mo–Mo reaction coordinate and the Mo–C reaction coordinate than the corresponding [Ar-CrCr-Ar] potential-energy surface.

Table 2. Most significant structural parameters and bond order for the [Ar-MM-Ar] systems.

System/Theory	M–M [Å]	M–C [Å]	M–C$_{aryl}$ [Å]	M-M-C [°]	C-M-M-C [°]	EBO/ Mayer BO[b]
[Ar-CrCr-Ar]/DFT	1.729	2.086	2.260	101.6	164.9	3.82
[Ar-CrCr-Ar]/CASPT2	1.836	2.132	2.258	99.2	180.0	3.07
[Ar-CrCr-Ar]/exptl[a]	1.8351(4)	2.131(1)	2.294(1)	102.78(1)	180[c]	
[Ar-MoMo-Ar]/DFT	2.464	2.142	2.304	112.9	124.0	3.85
[Ar-MoMo-Ar]/CASPT2	1.980	2.217	2.409	96.2	162.2	4.30
[Ar-WW-Ar]/DFT	2.419	2.160	2.374	104.6	134.9	3.25
[Ar-WW-Ar]/CASPT2	2.250	2.161	2.376	96.6	176.4	4.33

[a] From reference [19]. [b] Mayer bond order from DFT and EBO from CASPT2. [c] This angle is required to be 180° due to crystallographic symmetry.

 © 2012 Wiley-VCH Verlag GmbH & Co. KGaA, Weinheim

For **3c**, the DFT W–W bond length is 0.17 Å longer than the CASPT2 bond length. The occupation numbers for the natural orbitals (reported in Supporting Information) that make up the W–W bond provide an EBO of 4.3. Analogously to the prior cases, the closed shell configuration, $\sigma_g^2\pi_u^4\delta_g^4$, which corresponds to a formal quintuple bond, dominates the multideterminantal wavefunction with a weight of 69%.

A closer inspection of EBO values and weights of the dominating electronic configurations indicates that the magnitude of the M–M bond order goes as: Cr < Mo ≈ W, in agreement with the trend found for the simpler [Ph-MM-Ph] models and for the diatomic molecules.[14,39] The relative bond order is maintained along the series as Ph is replaced by Ar: the Mo–Mo and W–W bond orders are about one unit larger than the Cr–Cr bond order.

At the CASPT2 level the Cr–Cr bond is 0.08 Å longer in **3a** than in [Ph-CrCr-Ph], while the EBO remains the same. Steric encumbrance might be the reason for this bond lengthening. DFT predicts a larger effect on the Mo–Mo and W–W bonds due to the flanking aryl groups than does CASPT2.

The Burdzinski Mo–Mo system: The most significant structural parameters of our theoretical study on compound **1** (Figure 3), experimentally synthesized by Burdzinski et al.,[4] are reported in Table 3.

The DFT/PBE Mo–Mo distance is on the larger side of the experimental value, while the CASPT2 value is slightly smaller. The ground state is a singlet ^1A_g state. The wavefunction is dominated, about 75%, by the Hartree–Fock $\sigma_g^2\pi_u^4\delta_g^4$ configuration; the second most important configuration, about 7%, corresponds to a double excitation. natural orbitals and their occupation number are reported in Figure 6.

Table 3. Structural parameters and bond order for compound **1**.

Theory	Mo–Mo [Å]	M–O_{form}[b] [Å]	M–O [Å] [S-side]	M-O [Å] [non S-side]	Mo-Mo-O [°]	EBO/ Mayer BO[c]
DFT	2.168	2.105	2.087	2.082	91.6–91.8	3.44
CASPT2	2.068	2.107	2.089	2.084	93.0–93.2	3.40
exptl[a]	2.1032(6)	2.1093	2.1053	2.1033	90.9–92.8	

[a] From reference [4]. [b] O_{form}: oxygen atoms of the formate group. [c] Mayer bond order from DFT and EBO from CASPT2.

The EBO at the equilibrium bond length is equal to 3.4, which is very similar to the Mayer BO (3.44) calculated from DFT. In previous DFT calculations on this system,[4] the HOMO was found to be primarily of Mo_2 δ character, and the LUMO of Mo_2 δ* character. This description is supported by inspection of the natural orbital occupation numbers for the ground state.

The excitation energies for the lowest singlet and triplet states and their electronic configurations are reported in Table 4. Burdzinski et al.[4] performed time-dependent DFT calculations which predicted the lowest-energy electronic transitions of high intensity to correspond to Mo_2 δ→ligand π* and to move to lower energy with increasing number of rings. In the present study we determined only metal-based excitations because the orbitals included in the active space are exclusively metal based. The lowest Mo_2 δ→Mo_2 δ* singlet–singlet excitation is predicted to occur at 3.08 eV. The lowest singlet-triplet Mo_2 δ→Mo_2 δ* excitation occurs at 1.61 eV. These values are consistent with experimental data for Mo_2 carboxylates, which show δ–δ* transitions at about 2.85 eV.[52]

Table 4. Excitation energies for the lowest singlet and triplet states of compound **1** and their electronic configurations.

States		*E* [eV]	Configuration
S1	^1A_g	0	75% $\sigma^2\pi^4\delta^2$
T1	^3B_u	1.61	83% $\sigma^2\pi^4\delta^1\delta^{*1}$
S2	^1B_u	3.08	74% $\sigma^2\pi^4\delta^1\delta^{*1}$
T2	^3A_g	3.17	79% $\sigma^2\pi^3\delta^1\pi^{*1}$
T3	^3B_g	3.18	78% $\sigma^2\pi^4\delta^1\sigma^{*1}$
S4	^1B_g	3.62	83% $\sigma^2\pi^4\delta^1\sigma^{*1}$
S3	^1A_g	3.65	81% $\sigma^2\pi^4\delta^1\pi^{*1}$
T4	^3A_u	3.78	82% $\sigma^1\pi^4\delta^2\delta^{*1}$
S5	^1A_u	4.17	83% $\sigma^1\pi^4\delta^2\delta^{*1}$

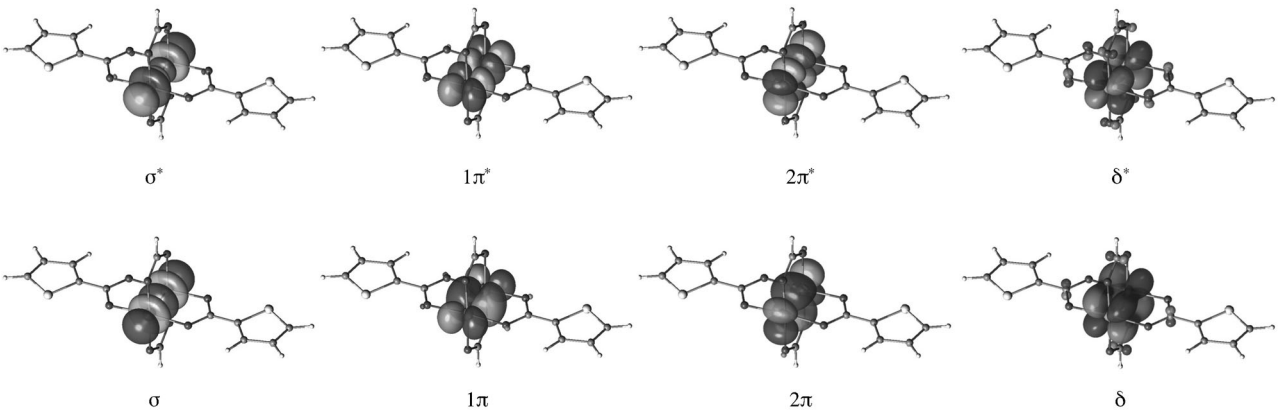

Figure 6. Natural orbitals for the ^1A_g ground state of compound **1**.

© 2012 Wiley-VCH Verlag GmbH & Co. KGaA, Weinheim

$[M_2(dpa)_4]$ (M = Cr, Mo, W) species: Initially, a DFT geometry optimization of $[Cr_2(dpa)_4]$ (**2a**) was performed starting from the experimental geometry. The calculated geometric parameters are shown in Table 5, where they are compared to experimental values. The optimized Cr–Cr distance, 1.91 Å is very close to the experimental value of 1.94 Å and the calculated Mayer bond order is 3.26. The DFT geometry optimization reproduces well the $Cr–N_a$ (2.05 Å), $Cr–N_{py}$ (2.07 Å), and the nonbonding Cr···N distances to the dangling pyridine groups (2.96 Å vs. experimental distances of 2.92 Å). Cotton and co-workers have defined a "direction angle" (ξ) as the angle between the pyridine plane and the $Cr–N_a$ bond vector, as a means of evaluating the degree of electron donation from the dangling pyridine lone pair into the Cr_2 π^* orbital.[53] As ξ deviates from 0°, lone-pair/π^* overlap diminishes due to misdirection of the pyridine group. The sum of the direction angles, $\Sigma\xi$, for **2a** is experimentally found in the range of about 100–120°, signifying little N lone-pair overlap with the Cr_2 π^* orbitals.[54] The geometry optimization slightly underestimates the observed $\Sigma\xi$ values at 81.2°. It is possible therefore that DFT may slightly overestimate electron delocalization between the free pyridine lone pairs and the Cr_2 unit. The long $Cr\cdots N_{py}$ distance of 2.96 Å suggests, however, that such electron delocalization will be minimal. CASPT2 single-point calculations were performed at the DFT-optimized geometry. The ground-state wavefunction is highly multiconfigurational leading to an EBO of 3.25. The $\sigma^2\pi^4\delta^2$ configuration is found to account for 36% of the ground state wavefunction. The second major contributing configuration $\pi^4\delta^2\delta^{*2}$ has a weight of 17%.

The electronic absorption spectrum of **2a** (Figure 7) is characterized by a single peak at 522 nm. TD-DFT calculations were performed at the optimized geometry predicting a singlet δ–δ* transition at 692 nm and two degenerate ligand-to-metal charge-transfer transitions at 554 nm (Figure 8). CASPT2 vertical excitation energies for the lowest singlet and triplet excited states with their intensities are reported in Table 6. In accordance with the multireference nature of **2a**, the lowest energy excitation to the triplet δ–δ* state is calculated to be only 0.61 eV (ca. 4900 cm^{-1}; 2000 nm) above the ground-state energy level. This transition is forbidden and has zero calculated intensity. The singlet σ^2–δ^{*2} state (S2) at 348 nm is also calculated to have essentially zero intensity, since it is essentially a two-electron

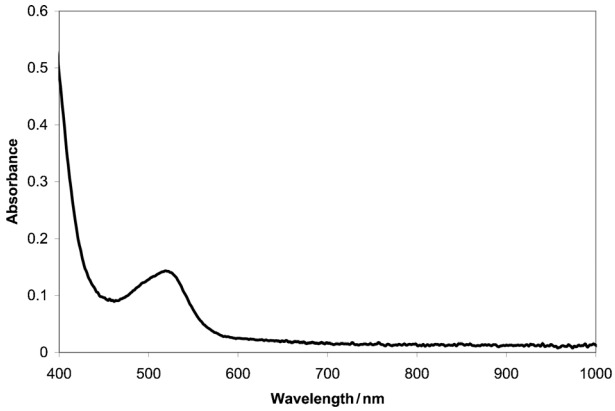

Figure 7. Electronic absorption spectrum of $[Cr_2(dpa)_4]$ (**2a**).

excitation. The higher energy excited states involve promotion of one of the σ electrons, though these bands are predicted in the UV and would not be observable due to concealment by charge transfer bands.

A DFT geometry optimization was performed on $[Mo_2(dpa)_4]$ **2b**, starting from the experimental geometry and then single-point energy calculations were performed at this optimized geometry at the CASPT2 level of theory. The optimized Mo–Mo bond length of 2.11 Å is in very good agreement with the experimentally determined distance of 2.10 Å. The calculated Mo–N bond lengths all agree with those determined crystallographically to within 0.01 Å. The calculated sum of the direction angles $\Sigma\xi = 101.8°$ also agrees very well with the experimental value of 104°. CASPT2 calculations reveal the ground-state wavefunction to be dominated by the closed-shell $\sigma^2\pi^4\delta^2$ electronic configuration, about 75%, leading to an EBO equal to 3.4. DFT predicts a slightly lower Mayer bond order of 3.0.

The electronic absorption spectrum of **2b** (see Supporting Information) is characterized by intense transitions at 585 and 500 nm, and higher energy, <400 nm, absorptions. TD-DFT calculations predict the singlet δ–δ* transition to be at 710 nm, which is unreasonably low in energy, and a doubly degenerate metal-to-ligand charge-transfer transition is predicted at 622 and 623 nm (Figure 8). The CASPT2 calculated absorption energies, with their intensities are reported in Table 7. The singlet δ–δ* transition is predicted to be at 431 nm.

Table 5. Calculated and experimental structural data for $[Cr_2(dpa)_4]$,[53] $[Mo_2(dpa)_4]$,[6] and $[W_2(dpa)_4]$.[5] Average values are reported for all structural data except for the M–M distance for which there is a unique value. Bond lengths in Å, dihedral angles in °.

	M–M	$M–N_a$	$M–N_{py}$	$M\cdots N_{py}$	N_a-M-M-N_{py}	M-N_a-C-N_{py}	$\Sigma\xi$	Mayer BO	EBO
2a DFT	1.914	2.052	2.069	2.96	18.8	20.3	81.2	3.26	3.25
2a exptl	1.943(2)	2.054(5)	2.068(5)	2.92(6)	5.1(2)	25.9(6)	104(3)	–	–
2a $2CH_2Cl_2$	1.940(1)	2.045(3)	2.074(3)	2.92(3)	7.4	30.9	124(2)	–	–
2b DFT	2.109	2.163	2.174	2.96	1.9	25.5	101.8	3.00	3.4
2b exptl	2.097(1)	2.166[3]	2.178[3]	2.97	3.4	26.05	104	–	–
2c DFT	2.241	2.173	2.175	2.92	1.0	24.7	98.8	2.98	–
2c CASPT2	2.251	2.159	–	–	–	–	–	–	3.52
2c exptl	2.1934(4)	2.132(5)	2.132(5)	2.932(5)	3.6(2)	26.7(5)	106.8	–	–

 © 2012 Wiley-VCH Verlag GmbH & Co. KGaA, Weinheim

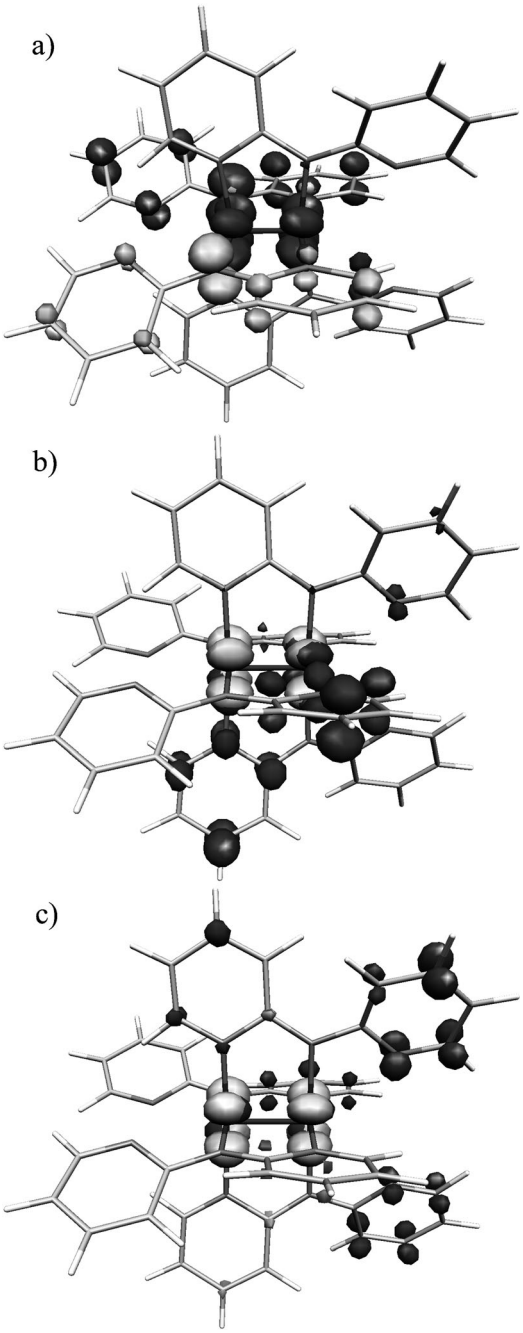

Figure 8. a) Ligand-to-metal charge-transfer orbitals for $[Cr_2(dpa)_4]$. b) Metal-to-ligand charge-transfer orbitals for $[Mo_2(dpa)_4]$. c) Metal-to-ligand charge-transfer orbitals for $[W_2(dpa)_4]$. Black represents donating orbitals. Gray represents accepting orbitals.

The electronic structure of $[W_2(dpa)_4]$ (**2c**) was investigated in a similar fashion. A DFT geometry optimization of **2c** was performed followed by a re-optimization of the W−W distance at the CASPT2 level of theory. The most significant structural parameters are reported in Table 5, where they are compared to experimental results. CASPT2 calculations reveal that the ground-state wavefunction is dominated by the $\sigma^2\pi^4\delta^2$ electronic configuration, about 76%, resulting in a EBO equal to 3.52. The Mayer BO calculated by DFT is lower at 2.98.

Table 6. Excitation energies from S1 (intensity in parentheses) in eV and nm for the lowest singlet and triplet states (in D_2 point group) and their electronic configurations for $[Cr_2(dpa)_4]$ (**2a**).

States		E [eV] (intensity)	E [nm]	Configuration
S1	^1A	0	0	36% $\sigma^2\pi^4\delta^2$
				17% $\pi^4\delta^2\delta^{*2}$
T1	$^3B_3$	0.61 (0)	2000	90% $\sigma^2\pi^4\delta^1\delta^{*1}$
S2	^1A	3.56 (0.2×10^{-6})	348	28% $\pi^4\delta^2\delta^{*2}$
				13% $\sigma^2\pi^4\delta^2$
				12% $\sigma^1\pi^4\delta^2\delta^{*1}$
T2	^3A	3.69 (0.7×10^{-5})	336	92% $\sigma^2\pi^4\delta^1\delta^{*1}$
S3	$^1B_3$	3.71 (0.2×10^{-3})	335	55% $\sigma^1\pi^4\delta^2\pi^{*1}$
S4	$^1B_3$	3.75 (0.2×10^{-3})	331	45% $\sigma^1\pi^4\delta^2\delta^{*1}$
S5	$^1B_1$	3.83 (0.2×10^{-4})	324	55% $\sigma^1\pi^4\delta^2\delta^{*1}$

Table 7. Excitation energies from S1 (intensity in parentheses) in eV and nm for the lowest singlet and triplet states and their electronic configuration for $[Mo_2(dpa)_4]$ (**2b**).

State		E [eV] (intensity)	E [nm]	Configuration
S1	^1A	0	0	75% $\sigma^2\pi^4\delta^2$
T1	^3A	1.3 (0)	955	80% $\sigma^2\pi^4\delta^1\delta^{*1}$
S2	^1A	2.88 (0.7×10^{-2})	431	73% $\sigma^2\pi^4\delta^1\delta^{*1}$
T2	^3A	3.23 (0)	384	82% $\sigma^2\pi^4\delta^1\delta^{*1}$
S3	^1A	3.45 (0)	360	82% $\sigma^2\pi^4\delta^1\delta^{*1}$

The vertical excitation energies for the lowest singlet and triplet excited states, with their intensities are reported in Table 8. Compound **2c** is characterized as having one broad absorption in the visible region at 610 nm and higher energy features, <400 nm (see Supporting Information for the spectrum). CASPT2 predicts the lowest δ–δ* transition, a singlet to triplet excitation, at 615 nm to be weakly intense due to spin-orbit coupling. The lowest singlet δ–δ* transition is predicted to be at 467 nm. Time-dependent DFT calculations performed on **2c** predict a singlet δ–δ* transition at 804 nm, and two degenerate metal to ligand charge transfer transitions at 726 nm (Figure 8).

Table 8. Excitation energies from the S1 (intensity in parentheses) in eV and nm for the lowest singlet and triplet states and their electronic configuration for $[W_2(dpa)_4]$ (**2c**).

State		E [eV] (intensity)	E [nm]	Configuration
S1	^1A	0	0	76% $\sigma^2\pi^4\delta^2$
T1	^3A	2.02 (0.1×10^{-6})	615	81% $\sigma^2\pi^4\delta^1\delta^{*1}$
S2	^1A	2.66 (0.1×10^{-1})	467	74% $\sigma^2\pi^4\delta^1\delta^{*1}$
S3	^1A	3.63 (0.7×10^{-5})	342	59% $\sigma^2\pi^4\delta^{*2}$
S4	^1B	3.65 (0.5×10^{-5})	340	46% $\sigma^2\pi^4\delta^1\pi^{*1}$
				34% $\sigma^2\pi^4\delta^1\pi^{*1}$
S5	^1B	3.67 (0.4×10^{-5})	338	39% $\sigma^2\pi^4\delta^1\pi^{*1}$
				47% $\sigma^2\pi^4\delta^1\pi^{*1}$

The U−U hypothetical compound: The $[Cr_2(dpa)_4]$, $[Mo_2(dpa)_4]$, and $[W_2(dpa)_4]$ compounds (**2a–c**) were each made experimentally. We consider now, however, the U−U compound **2d** analogous to **2a–c**, which has not been synthe-

 © 2012 Wiley-VCH Verlag GmbH & Co. KGaA, Weinheim

sized. If good computational results on this hypothetical U_2 molecule can be obtained, then it may be reasonable to suggest this molecule as an interesting new target for synthetic chemists. Thus, we decided to perform a full electronic characterization of this species in order to see how different this species is from the analogous Cr–Cr, Mo–Mo, and W–W compounds and what are the chances that it may exist from an electronic structure point of view. We started from the X-ray coordinates of **2c** and replaced the two W atoms with two U atoms. Initially, DFT single-point energy calculations were performed for singlet, triplet, and quintet spin states to establish the nature of the ground state. The triplet was found to be the lowest energy spin state, with the quintet lying 0.2 eV higher and the singlet 0.6 eV higher in energy. A full geometry optimization of the triplet electronic state was performed at the DFT/PBE/SDD level of theory. At the triplet-optimized geometry single-point energy calculations for various spin states were performed at the CASSCF/CASPT2 level of theory using an active space of twelve electrons in twelve orbitals. These orbitals are linear combinations of U 6d and 5f orbitals and ligand-based orbitals of the appropriate symmetry to bind with these U orbitals. The ^{3}A state is the ground state as determined by DFT and also at the CASPT2 level of theory. Calculations with 14 electrons in 14 active space orbitals confirmed these results. We then optimized the U–U distance at the CASPT2 level of theory for both the singlet and triplet state. The general features of the DFT- and CASPT2-optimized structures of **2d** are similar to each other, and differ slightly from those of **2a–c**. Whereas the Cr_2, Mo_2, and W_2 compounds each contain a dangling pyridine ring from each dpa ligand that does not coordinate to the metal centers, all of the dpa N atoms bind to one U atom or the other in **2d**. Thus, the dpa ligand assumes an unusual bridging/chelating coordinate mode in **2d** (Scheme 2). Other reported examples of this coordination mode are found in the $[W_2(dpa)_3X_2]^+$,[5] $[W_2(dpa)_4]^{2+}$,[55] and the Ru_2[56] and V_2[57] analogues of these compounds. Some of the bond lengths in **2d** vary as a function of the spin state (Table 9). The U–N_a bond and U–N_{py} bond to the non-chelating pyridine moiety are, however, almost invariant at about 2.40 and 2.52 Å, respectively. The two U atoms are clearly close enough to each other in this molecule to be considered bonded to one another. In the triplet ground state, an U–U distance of 2.38 Å is calculated, which increases to 2.44 Å in the singlet state. In the triplet state, the U–N distance to the chelating pyridine ligands is 2.58 Å, indicating a significant interaction. In support of this conclusion, the sum of the direction angles, $\Sigma\xi$, of 66.8° is far smaller than in **2a–c**. This U–N bond becomes even shorter in the singlet state, in which it is found to be 2.48 Å, which is approximately 0.05 Å shorter than the U–N bond to the bridging pyridyl moiety. There is a concomitant decrease in $\Sigma\xi$ to 30° in the singlet state.

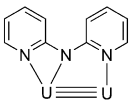

Scheme 2.

Table 9. Calculated structural data for $[U_2(dpa)_4]$ (**2d**). Average values are reported for all structural data except for the U–U distance for which there is a unique value. Bond lengths in Å, dihedral angles in °.

	U–U	U–N_a	U–N_{py}	U···N_{py}	N_a-U-U-N_{py}	ξ [°]	$\Sigma\xi$ [°]
triplet, DFT	2.38	2.42	2.52	2.58	5.4	16.7	66.8
singlet, DFT	2.44	2.40	2.53	2.48	16.2	7.4	29.6

Unlike **3a–c**, which feature M_2^{4+} units having a formal quadruple bond between the metal atoms, the electronic structure of the U_2 compound is different in that there are only six U_2-based electrons. This situation indicates that this compound contains a U^{III}–U^{III} dimer and therefore that two electrons are added to the ligand orbitals formally reducing the two dpa^- ligands to radical dianions. From a chemical viewpoint, this electron disposition is sensible, as U^{2+} would be expected to be highly reducing and, to our knowledge, no U^{2+} complexes have been reported. This result suggests that the corresponding dication $[U_2(dpa)_4]^{2+}$ may be a more realistic synthetic target. The EBO calculated for the singlet state of **2d** is equal to 2.1 at a U–U bond length of 2.47 Å. This value corresponds to a formal U_2^{6+} triple bond arising from the dominating electronic configuration $\sigma^2\pi^4$ (see Supporting Information for the details of the occupation numbers) This result should be compared with the one for the analogous $[Cr_2(dpa)_4]$, $[Mo_2(dpa)_4]$, and $[W_2(dpa)_4]$ compounds. In compound **2c** the W–W bond length for the singlet ground state is equal to 2.225 Å and in compound **2b** the Mo–Mo distance is 2.109 Å, corresponding to an EBO of 3.5 and 3.4, respectively. The U–U compound has a U–U bond one unit lower than the corresponding $[Mo_2(dpa)_4]$ and $[W_2(dpa)_4]$ compounds, consistent with the U_2^{6+} oxidation state.

Discussion

Compounds with metal–metal multiple bonds have consistently posed a considerable challenge to electronic structure calculations. The earliest reported methods that provided useful results utilized the SCF-Xα-SW method, though this method has been superseded in recent years by DFT methods.[2] The main failing of Hartree–Fock based computations on metal–metal multiply bonded compounds, especially on dichromium compounds, is the problem of electron correlation in systems in which many orbitals are energetically very closely spaced.[58,59] To some extent, this problem is ameliorated by DFT methods though it remains when hybrid functionals such as B3LYP or PBE0 are utilized,[60,61] but another problem inherent in DFT arises. Most density functionals within the Kohn–Sham approach have difficulties describing situations which are of multi-reference character in wavefunction based methods. For metal–metal multiply bonded compounds, the orbital energy separations are often small and several limiting electron configurations may contribute

 © 2012 Wiley-VCH Verlag GmbH & Co. KGaA, Weinheim

to the true ground-state wavefunction that must be described as a combination of multiple determinants.

The multireference method employed here, CASPT2, can describe, for the selected active space of electrons and orbitals, multiconfigurational electronic states. In this study on several different types of recently reported metal–metal multiply bonded molecules, we have employed both DFT and CASPT2 to compare calculated geometries and electronic excited states. Thus, it is now possible to provide a detailed assessment of the use of DFT versus multireference methods in treating metal–metal multiply bonded compounds. We will first discuss the computational results on molecular geometries obtained from DFT and CASSCF/CASPT2 and different assessments of metal–metal bond orders such as the Mayer bond order implemented in DFT and the EBO used with multireference wavefunctions. The electronic excited states will then be discussed.

DFT and CASPT2 geometry optimizations have been performed on the systems under examination. Since at the CASPT2 level, only selected bond lengths (metal–metal and metal–nearest-neighbor) were re-optimized, it makes sense only to discuss the metal–metal bond lengths in detail. For most molecules there was less than 0.1 Å difference between the DFT and CASPT2-optimized metal–metal bond lengths. The [Ar-MM-Ar] systems, however, showed the biggest disparity. The greatest difference is 0.48 Å for the metal–metal distance in the [Ar-MoMo-Ar] molecule, due to the formation of an η^6 interaction between the Mo and Aryl fragments in the DFT optimization. Despite the reasonable geometries provided by DFT for Cr_2, Mo_2, and W_2 compounds, prediction of spectral properties are not nearly as accurate.

To better understand the electronic absorption spectra of the Group 6 compounds $[Cr_2(dpa)_4]$, $[Mo_2(dpa)_4]$, and $[W_2(dpa)_4]$, TD-DFT was used in conjugation with CASPT2. The reason for employing both methods is that, while CASPT2 is more accurate than TD-DFT, because of its multiconfigurational nature, it can describe only those transitions generated by the orbitals present in the active space. In our calculations we could only include metal-based orbitals in the active space, because otherwise the active space would have become prohibitively large and it was thus not possible to predict the metal-to-ligand (ML) or ligand-to-metal (LM) charge-transfer (CT) transitions at the CASPT2 level.

The absorption spectrum for $[Cr_2(dpa)_4]$ is characterized by an absorption at 520 nm with molar absorptivity $4500\,M^{-1}cm^{-1}$ and higher energy transitions (<400 nm) that have yet to be unambiguously assigned. TD-DFT results predict the lowest singlet δ–δ* transition to be at 692 nm and two degenerate LMCT bands at 554 nm, involving promotion of an electron from a doubly occupied, delocalized dpa π orbital to the Cr–Cr δ* level. The lowest singlet transition predicted by CASPT2 calculations at 350 nm is notably not a δ–δ* transition, but is instead a two-electron excitation. Notably, TD-DFT significantly underestimates all of the excited state energies, as evidenced by the fact that there are no experimental absorptions where TD-DFT predicts them to be. However, the fact that TD-DFT predicts charge transfer bands in the visible region of the spectrum is significant. Considering all these results we assign the major absorption at 520 nm to be a LMCT band. The δ–δ* transition is likely present but cannot be directly observed as it is covered by the CT bands. TD-DFT is useful to assign the major feature of this spectrum as LMCT excitations, since these cannot be predicted by CASPT2.

The absorption spectrum of $[Mo_2(dpa)_4]$ is quite different from that of its Cr and W analogues. Two absorption bands are detected in the visible region at 500 and 585 nm. As per the discussion above, TD-DFT predicts both these peaks to be MLCT transitions, while CASPT2 predicts the singlet δ–δ* transition to occur at 431 nm, which would be covered by the CT bands in the absorption spectrum. The CASPT2 prediction of the δ–δ* transition at 431 nm is reasonable considering the energies of definitively assigned δ–δ* transitions in the dimolybdenum tetracarboxylates, which appear at about 430 nm.[2] As in the Cr_2 case, TD-DFT poorly predicts the energy of this band at 702 nm, a region in which the experimental spectrum is empty.

The absorption spectrum of $[W_2(dpa)_4]$ is characterized by a broad peak at 610 nm, which is assigned to be due to a combination of MLCT bands, based on TD-DFT results. CASPT2 calculations predict the singlet δ–δ* transition to be at 467 nm, considerably higher in energy than TD-DFT (804 nm). The δ–δ* transition is once again not observed due to the CT bands, and the CASPT2 δ–δ* transition is more physically reasonable than the TD-DFT result.

For $[Cr_2(dpa)_4]$ the charge transfer bands are predicted to be LMCT as opposed to the MLCT bands predicted for $[Mo_2(dpa)_4]$ and $[W_2(dpa)_4]$. At this point we do not fully understand why the direction of the charge transfer changes in these molecules, but we note that chemical oxidation of $[Mo_2(dpa)_4]$ and $[W_2(dpa)_4]$ to their respective monocations has been established experimentally,[5,53] whereas oxidation of $[Cr_2(dpa)_4]$ leads to decomposition.

The results reported here emphasize the importance of analyzing electronic absorption spectra using both TD-DFT and CASPT2 methods. It should be noted that CASPT2 calculations including the ligand orbitals in the active space would provide the best assessment of the absorption spectrum, but this task is currently prohibitively expensive.

The final point of discussion involves bond orders for metal–metal bonds. Basic molecular orbital theory, in which metal–metal bonding and antibonding orbitals may be occupied by either 0, 1, or 2 electrons, yields simple, integer bond orders for compounds **3** (bond order of 5), and **1** and **2** (bond orders of 4). These are the bond orders that stem from a zero-th order assessment of metal oxidation states and orbital overlap. Calculated bond orders are different from these simple MO bond orders for three main reasons: 1) metal–ligand delocalization, 2) non-ideal metal–metal orbital overlap, and 3) multiconfigurational states. The MO bond orders are therefore an upper limit for the number of electron pairs that hold two metals together, and calculated bond orders are always lower than these idealized values.

 © 2012 Wiley-VCH Verlag GmbH & Co. KGaA, Weinheim

In this work, we have presented two types of calculated bond orders. First, DFT results have been analyzed using the Mayer BO,[62] which is an extension of the Wiberg bond index used by semiempirical methods,[63] and results directly from Mulliken analysis of the wavefunction. For the multireference calculations presented here, the EBO method is used, which involves a summation of the bonding and antibonding orbital population for those orbitals in the active space. There are advantages and disadvantages to both methods. The Mayer BO may accurately reflect metal–ligand delocalization and imperfect metal–metal orbital overlap, but, since DFT is an inherently mono-determinantal method, multiconfigurational character of the wavefunction is ignored. The EBO method, on the other hand, deals exclusively with the multiconfigurational nature of the wavefunction, and thereby deals correctly with the issue of poor orbital overlap. However, since ligand orbitals are not included in the active space, metal–ligand delocalization is not reflected in this value.

It may be naively expected that the metal–metal bond order of a molecule correlates with the bond length. In general this is the case, though there are a number of notable counter examples. For instance, the first quintuply-bonded molecule, synthesized by Power and co-workers,[22] has a longer Cr−Cr bond length (1.84 Å) than that of the shortest quadruple bond (1.83 Å).[64] Also, in electron-rich metal–metal multiply bonded systems, metal–metal bond lengths can be affected more by electron-electron repulsion and other charge considerations than by changes in metal–metal bond order.[65–69] Nevertheless, comparisons between bond lengths and bond orders for the compounds presented here are enlightening. The formal shortness ratio (FSR)[2] will be used here in comparing bond lengths between metals of different sizes. FSR values for all of the compounds studied here are given in Table 10, along with FSR values for optimized geometries and the Mayer bond order and EBO values.

Table 10. Comparison of FSRs and calculated bond orders.

	Exptl FSR	DFT FSR	CASPT2 FSR	Mayer BO	EBO
1	0.811	0.836	0.798	3.44	3.40
2a	0.819	0.752	–	3.26	3.25
2b	0.809	0.814	–	3.10	3.40
2c	0.841	0.848	0.863	2.98	3.50
2d	–	0.856	0.866	–	2.1
3a	0.774	0.729	0.774	3.82	3.07
3b	–	0.951	0.734	3.85	4.30
3c	–	0.928	0.863	3.25	4.33

All of the compounds presented here that have been characterized expermentally have FSR values significantly less than one, consistent with metal–metal multiple bonding. The lowest FSR of 0.774 belongs to the quintuply bonded molecule **3a**. All of the quadruply bonded molecules have FSR values in the range of 0.809-0.841. The agreement between FSR values calculated from DFT or CASPT2 methods and the experimental FSRs mirrors the agreement between optimized and measured metal–metal bond lengths.

Our simplistic general expectation is that compounds having a smaller FSR should have larger bond orders, since these are the species whose metal–metal separations deviate most from the sum of the metallic radii. A correlation of bond order with FSR is shown in Figure 9, using only the

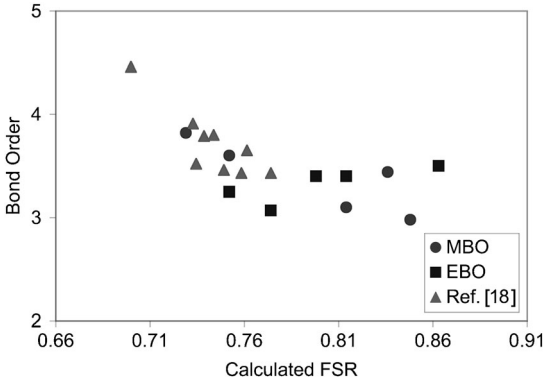

Figure 9. Correlation plot of bond order with formal shortness ratio.

data from Table 10 for real compounds that have been analyzed by both DFT and multireference methods (that is, **3a**, **1**, **2a**, **2b**, and **2c**). EBO data for "supershort" Cr_2 compounds reported in reference [18] are also included. Compounds **3b** and **3c** are not included in this analysis. Their calculated EBO values are anomalously high because the active space orbitals are not purely metal orbitals but contain significant ligand character due to arene–metal π interactions. Taking into account all of the available data, we see that, indeed the calculated bond orders (both Mayer BO and EBO) generally increase as the normalized metal–metal bonds become shorter. Some subtleties are worth pointing out, however. A somewhat counter intuitive result is the fact that the EBO values increase for the compounds studied here as the metal is changed from Cr to Mo or W, despite the fact that the Mo_2 and W_2 molecules have higher FSR values. This result can be rationalized by considering that the 4d (Mo) or 5d (W) orbitals are significantly larger than the Cr 3d orbitals. One may therefore expect Mo_2 and W_2 molecules to have greater orbital overlap, and hence larger computed bond orders, at longer normalized bond lengths than for the Cr_2 molecules.

It is unclear from the current set of data whether DFT bond orders also show this effect. This analysis of calculated bond orders as a function of metal–metal bond lengths should be considered with the following caveats in mind. Metal–metal bond lengths can be affected by steric factors such as the bite angle of the bridging ligands. Electronic factors can also be important. For example, increased covalency of metal–carbon bonds can affect the calculated bond orders. Local symmetry may also be important, as it can lead to more polarized metal–metal interactions. Despite these complicating factors, both MBO and EBO bond order

 © 2012 Wiley-VCH Verlag GmbH & Co. KGaA, Weinheim

metrics show the anticipated trend with bond length. The agreement between the MBO and EBO metrics in this trend is remarkable, given the shortcomings of each method enumerated above.

Conclusion

We have reported the results of a study of several Cr–Cr, Mo–Mo, and W–W compounds with different ligands and formal metal oxidation states. We have investigated the Mo and W analogue of the recently synthesized [Ar-CrCr-Ar] compound **3a**. The effect of Ar on the different bimetallic units has been compared with the effect of Ph in the analogous [Ph-MM-Ph] compounds. The metal–metal effective bond order obtained from the occupation numbers of the natural orbitals resulting from the CASSCF wavefunction is close to five in [Ph-MoMo-Ph] and [Ph-WW-Ph], while it is only close to four in [Ph-CrCr-Ph]. The EBO remains substantially invariant in the [Ar-MM-Ar] compounds, compared to the Ph analogues, indicating that the flanking aryl groups have mainly a steric effect, rather than an electronic one.

Compounds **1** and **2a–c**, which contain formal quadruple bonds between Cr_2, Mo_2, and W_2 units, have also been investigated. Finally, the hypothetical U–U molecule $[U_2(dpa)_4]$ is described as an $U_2^{III,III}$ compound, with a formal U_2 triple bond, and two dpa ligands reduced to radical anions. We have also computed the lowest energy excited states of **1** and **2a–c** using both CASPT2 (for metal–metal excitations) and TD-DFT (for metal–ligand charge-transfer excitations). These combined methods allow us to assign the major features of the absorption spectra of **1** and **2a–c** as charge transfer bands, which cover up the δ–δ* transitions that would otherwise be observed.

These results indicate that in general the Cr–Cr bond is more multiconfigurational than the Mo–Mo and W–W in analogous compounds leading to lower calculated EBO values. As already described in the case of the diatomics, the reason should be attributed to the more favorable interaction between the d orbitals for second- and third-row transition metals compared with first-row transition metals. It is interesting to note that, for the same metal, the bond order is similar in the [Ar-MM-Ar] (M = Cr, Mo, W), [MM′-(TiPB)$_4$] (M = Mo, W; M′ = W) and [M_2(dpa)$_4$] (M = Mo,W) compounds.

Comparing calculated bond orders to normalized bond lengths using the formal shortness ratio (FSR), we see that both Mayer bond orders, calculated from DFT methods, and effective bond orders, from CASSCF calculations, provide comparable reliability with respect to their correlation with FSR. Taking this result together with the results of excited state calculations reported here, there are clear advantages to the combined use of both DFT and multireference methods in describing compounds with the metal–metal multiple bonds.

We plan to study oligomeric species containing several of these units in order to explore the trend of the metal–metal multiple bonds for growing oligomers. We will also investigate the effect of the length of the thienyl groups on the CASSCF wavefunction and subsequent electronic properties of compounds of type **1**.

Acknowledgements

We thank the Office of Basic Energy Sciences, U. S. Department of Energyunder Contract no. USDOE/DE-SC002183 for financial support and the University of Minnesota Supercomputing Institute. The National Science Foundationis gratefully acknowledged for support under CHE-0745500.

[1] F. A. Cotton, C. B. Harris, *Inorg. Chem.* **1965**, *4*, 330.
[2] F. A. Cotton, C. A. Murillo, R. A. Walton, *Multiple Bonds Between Metal Atoms*, 3rd ed., Springer: Berlin, **2005**.
[3] B. G. Alberding, M. H. Chisholm, Y. H. Chou, J. C. Gallucci, Y. Ghosh, T. L. Gustafson, N. J. Patmore, C. R. Reed, C. Turro, *Inorg. Chem.* **2009**, *48*, 4394.
[4] G. T. Burdzinski, M. H. Chisholm, P. T. Chou, Y. H. Chou, F. Feil, J. C. Gallucci, Y. Ghosh, T. L. Gustafson, M. L. Ho, Y. Liu, R. Ramnauth, C. Turro, *Proc. Natl. Acad. Sci. USA* **2008**, *105*, 15247.
[5] M. Nippe, E. Victor, J. F. Berry, *Inorg. Chem.* **2009**, *48*, 11889.
[6] M. C. Suen, Y. Y. Wu, J. D. Chen, T. C. Keng, J. C. Wang, *Inorg. Chim. Acta* **1999**, *288*, 82.
[7] M. Nippe, J. F. Berry, *J. Am. Chem. Soc.* **2007**, *129*, 12684.
[8] M. Nippe, E. Victor, J. F. Berry, *Eur. J. Inorg. Chem.* **2008**, 5569.
[9] M. Nippe, G. H. Timmer, J. F. Berry, *Chem. Commun.* **2009**, 4357.
[10] M. Nippe, J. F. Wang, E. Bill, H. Hope, N. S. Dalal, J. F. Berry, *J. Am. Chem. Soc.* **2010**, *132*, 14261.
[11] D. Aydin-Cantürk, H. Nuss, *Z. Anorg. Allg. Chem.* **2011**, *637*, 543.
[12] G. Cavigliasso, N. Kaltsoyannis, *Dalton Trans.* **2006**, 5476.
[13] G. Cavigliasso, N. Kaltsoyannis, *Inorg. Chem.* **2007**, *46*, 3557.
[14] B. O. Roos, A. C. Borin, L. Gagliardi, *Angew. Chem.* **2007**, *119*, 1491; *Angew. Chem. Int. Ed.* **2007**, *46*, 1469.
[15] M. Brynda, L. Gagliardi, P. O. Widmark, P. P. Power, B. O. Roos, *Angew. Chem.* **2006**, *118*, 3888; *Angew. Chem. Int. Ed.* **2006**, *45*, 3804.
[16] B. O. Roos, P. Linse, P. E. M. Siegbahn, M. R. A. Blomberg, *Chem. Phys.* **1982**, *66*, 197.
[17] B. O. Roos, *Collect. Czech. Chem. Commun.* **2003**, *68*, 265.
[18] G. La Macchia, G. Li Manni, T. K. Todorova, M. Brynda, F. Aquilante, B. O. Roos, L. Gagliardi, *Inorg. Chem.* **2010**, *49*, 5216.
[19] T. Nguyen, A. D. Sutton, M. Brynda, J. C. Fettinger, G. J. Long, P. P. Power, *Science* **2005**, *310*, 844.
[20] C. R. Landis, F. Weinhold, *J. Am. Chem. Soc.* **2006**, *128*, 7335.
[21] G. La Macchia, L. Gagliardi, P. P. Power, M. Brynda, *J. Am. Chem. Soc.* **2008**, *130*, 5104.
[22] T. Nguyen, A. Panda, M. M. Olmstead, A. F. Richards, M. Stender, M. Brynda, P. P. Power, *J. Am. Chem. Soc.* **2005**, *127*, 8545.
[23] T. Nguyen, W. A. Merrill, C. Ni, H. Lei, J. C. Fettinger, B. D. Ellis, G. L. Long, M. Brynda, P. P. Power, *Angew. Chem.* **2008**, *120*, 9255; *Angew. Chem. Int. Ed.* **2008**, *47*, 9115.
[24] L. Gagliardi, B. O. Roos, *Chem. Soc. Rev.* **2007**, *36*, 893.
[25] B. O. Roos, L. Gagliardi, *Inorg. Chem.* **2006**, *45*, 803.
[26] L. Gagliardi, P. Pyykko, B. O. Roos, *Phys. Chem. Chem. Phys.* **2005**, *7*, 2415.
[27] R. Ahlrichs, M. Bar, M. Haser, H. Horn, C. Kolmel, *Chem. Phys. Lett.* **1989**, *162*, 165.
[28] J. P. Perdew, A. Zunger, *Phys. Rev. B* **1981**, *23*, 5048.
[29] B. O. Roos, P. R. Taylor, P. E. M. Siegbahn, *Chem. Phys.* **1980**, *48*, 157.

 © 2012 Wiley-VCH Verlag GmbH & Co. KGaA, Weinheim

[30] K. Andersson, P.-. Malmqvist, B. O. Roos, *J. Chem. Phys.* **1992**, *96*, 1218.
[31] F. Aquilante, L. De Vico, N. Ferré, G. Ghigo, P.-. Malmqvist, T. Pedersen, M. Pitonak, M. Reiher, B. O. Roos, L. Serrano-Andrés, M. Urban, V. Veryazov, R. Lindh, *J. Comput. Chem.* **2010**, *31*, 224.
[32] B. O. Roos, R. Lindh, P. A. Malmqvist, V. Veryazov, P. O. Widmark, *J. Phys. Chem. A* **2005**, *109*, 6575.
[33] B. O. Roos, R. Lindh, P. A. Malmqvist, V. Veryazov, P. O. Widmark, *J. Phys. Chem. A* **2004**, *108*, 2851.
[34] B. A. Hess, *Phys. Rev. A* **1986**, *33*, 3742.
[35] F. Aquilante, T. B. Pedersen, R. Lindh, *J. Chem. Phys.* **2007**, *126*, 194106.
[36] F. Aquilante, P. A. Malmqvist, T. B. Pedersen, A. Ghosh, B. O. Roos, *J. Chem. Theory Comput.* **2008**, *4*, 694.
[37] F. Aquilante, T. B. Pedersen, R. Lindh, B. O. Roos, A. S. De Meras, H. Koch, *J. Chem. Phys.* **2008**, *129*, 024113.
[38] F. Aquilante, T. K. Todorova, L. Gagliardi, T. B. Pedersen, B. Roos, *J. Chem. Phys.* **2009**, *131*, 034113.
[39] M. Brynda, L. Gagliardi, B. O. Roos, *Chem. Phys. Lett.* **2009**, *471*, 1.
[40] F. Weinhold, C. R. Landis, *Science* **2007**, *316*, 61.
[41] A. E. Reed, L. A. Curtiss, F. Weinhold, *Chem. Rev.* **1988**, *88*, 899.
[42] F. R. Wagner, A. Noor, R. Kempe, *Nat. Chem.* **2009**, *1*, 529.
[43] L. Gagliardi, B. O. Roos, *Inorg. Chem.* **2003**, *42*, 1599.
[44] F. Ferrante, L. Gagliardi, B. E. Bursten, A. P. Sattelberger, *Inorg. Chem.* **2005**, *44*, 8476.
[45] F. Poineau, L. Gagliardi, P. M. Forster, A. P. Sattelberger, K. R. Czerwinski, *Dalton Trans.* **2009**, 5954.
[46] F. Poineau, P. M. Forster, T. K. Todorova, L. Gagliardi, A. P. Sattelberger, K. R. Czerwinski, *Inorg. Chem.* **2010**, *49*, 6646.
[47] Gaussian 09, Revision B.01, M. J. Frisch, G. W. Trucks, H. B. Schlegel, G. E. Scuseria, M. A. Robb, J. R. Cheeseman, G. Scalmani, V. Barone, B. Mennucci, G. A. Petersson, H. Nakatsuji, M. Caricato, X. Li, H. P. Hratchian, A. F. Izmaylov, J. Bloino, G. Zheng, J. L. Sonnenberg, M. Hada, M. Ehara, K. Toyota, R. Fukuda, J. Hasegawa, M. Ishida, T. Nakajima, Y. Honda, O. Kitao, H. Nakai, T. Vreven, J. A. Montgomery, Jr., J. E. Peralta, F. Ogliaro, M. Bearpark, J. J. Heyd, E. Brothers, K. N. Kudin, V. N. Staroverov, R. Kobayashi, J. Normand, K. Raghavachari, A. Rendell, J. C. Burant, S. S. Iyengar, J. Tomasi, M. Cossi, N. Rega, J. M. Millam, M. Klene, J. E. Knox, J. B. Cross, V. Bakken, C. Adamo, J. Jaramillo, R. Gomperts, R. E. Stratmann, O. Yazyev, A. J. Austin, R. Cammi, C. Pomelli, J. W. Ochterski, R. L. Martin, K. Morokuma, V. G. Zakrzewski, G. A. Voth, P. Salvador, J. J. Dannenberg, S. Dapprich, A. D. Daniels, Ö. Farkas, J. B. Foresman, J. V. Ortiz, J. Cioslowski, D. J. Fox, Gaussian, Inc., Wallingford CT, **2009**.
[48] S. I. Gorelsky, A. B. P. Lever, *J. Organomet. Chem.* **2001**, *635*, 187.
[49] S. I. Gorelsky, University of Ottawa, **2011**.
[50] P. . Malmqvist, *Int. J. Quantum Chem.* **1986**, *30*, 479.
[51] B. O. Roos, P. A. Malmqvist, *Phys. Chem. Chem. Phys.* **2004**, *6*, 2919.
[52] D. S. Martin, R. A. Newman, P. E. Fanwick, *Inorg. Chem.* **1979**, *18*, 2511.
[53] F. A. Cotton, G. Wilkinson, C. A. Murillo, M. Bochmann, *Advanced Inorganic Chemsitry*; 6th ed.; Wiley: New York, **1999**.
[54] F. A. Cotton, L. M. Daniels, C. A. Murillo, I. Pascual, H.-C. Zhou, *J. Am. Chem. Soc.* **1999**, *121*, 6856.
[55] M. Nippe, S. M. Goodman, C. G. Fry, J. F. Berry, *J. Am. Chem. Soc.* **2011**, *133*, 2856.
[56] J. F. Berry, F. A. Cotton, C. A. Murillo, *Inorg. Chim. Acta* **2004**, *357*, 3847.
[57] F. A. Cotton, L. M. Daniels, C. A. Murillo, H. C. Zhou, *Inorg. Chim. Acta* **2000**, *305*, 69.
[58] M. B. Hall, *Polyhedron* **1987**, *6*, 679.
[59] P. M. Atha, I. H. Hillier, A. A. Macdowell, M. F. Guest, *J. Chem. Phys.* **1982**, *77*, 195.
[60] C. J. Cramer, D. G. Truhlar, *Phys. Chem. Chem. Phys.* **2009**, *11*, 10757.
[61] G. H. Timmer, J. F. Berry, *C. R. Chim.* **2011**, DOI: 10.1016/j.crci.2011.09.001, in press.
[62] I. Mayer, *Chem. Phys. Lett.* **1983**, *97*, 270.
[63] K. B. Wiberg, *Tetrahedron* **1968**, *24*, 1083.
[64] F. A. Cotton, S. A. Koch, M. Millar, *Inorg. Chem.* **1978**, *17*, 2084.
[65] J. F. Berry, E. Bill, E. Bothe, F. A. Cotton, N. S. Dalal, S. A. Ibragimov, N. Kaur, C. Y. Liu, C. A. Murillo, S. Nellutla, J. M. North, D. Villagran, *J. Am. Chem. Soc.* **2007**, *129*, 1393.
[66] F. A. Cotton, K. R. Dunbar, L. R. Falvello, M. Tomas, R. A. Walton, *J. Am. Chem. Soc.* **1983**, *105*, 4950.
[67] B. E. Bursten, F. A. Cotton, P. E. Fanwick, G. G. Stanley, R. A. Walton, *J. Am. Chem. Soc.* **1983**, *105*, 2606.
[68] P. A. Koz′min, T. B. Larina, M. D. Surazhskaya, *Russ. J. Coord. Chem.* **1982**, *8*, 451.
[69] F. A. Cotton, L. D. Gage, *Nouv. J. Chim.* **1977**, *1*, 441.

Received: October 4, 2011
Published online: January 11, 2012

 © 2012 Wiley-VCH Verlag GmbH & Co. KGaA, Weinheim